coatings

Article

Effect of Ultrasonic Treatment on Microstructure and Properties of 2000 MPa Ultra-High-Strength Steel-Welded Joints

Qibao Chu [1], Gang Wang [2], Ren Yuan [3,*] and Xiangyu Xu [2]

[1] Nuclear and Radiation Safety Center of the Ministry of Ecology and Environment, Beijing 100082, China; chuqibao2005@126.com
[2] State Key Laboratory of Advanced Welding and Joining, Harbin Institute of Technology, Harbin 150001, China; 18253312631@163.com (G.W.); 23b9090173@stu.hit.edu.cn (X.X.)
[3] Intelligent Manufacturing System Engineering Center, College of Creative Arts, Shanghai Tech University, Shanghai 201210, China
* Correspondence: nb1020627395@outlook.com

Abstract: The microstructure and mechanical properties of ultra-high-strength steel weld joints were examined for the effect of ultrasonic treatment. ER120S-G welding wire is necessary for welding 4 mm thick ultra-high-strength steel. After that, the weld toe region underwent different parameters of the ultrasonic stress relief process. As a means of surface treatment for weld seams, noticeable grain refinement and the formation of a fine-grained layer were observed in the weld toe region after ultrasonic treatment. The blind hole method was used to measure residual stresses in the weld seam, which indicated a transition from tensile stress to compressive stress in the treated portion of the joint. Different ultrasonic treatment processes resulted in a significant increase in hardness values near the weld toe region during hardness testing. The hardness of the weld joint that was treated with ultrasound increased initially but then stabilized after increasing the frequency. The ultrasound-treated joints showed a significant improvement in both tensile strength and fracture elongation, as demonstrated in the tensile tests.

Keywords: 2000 MPa ultra-high-strength steel; ultrasonic treatment; weld residual stress; microstructure; mechanical properties

check for updates

Citation: Chu, Q.; Wang, G.; Yuan, R.; Xu, X. Effect of Ultrasonic Treatment on Microstructure and Properties of 2000 MPa Ultra-High-Strength Steel-Welded Joints. *Coatings* **2023**, *13*, 1995. https://doi.org/10.3390/coatings13121995

Academic Editors: Ramachandran Chidambaram Seshadri and A.K. Lakshminarayanan

Received: 4 November 2023
Revised: 22 November 2023
Accepted: 23 November 2023
Published: 24 November 2023

1. Introduction

The strength, hardness, and toughness of the new ultra-high-strength steel produced has significantly improved since the continuous improvement of steel smelting and since rolling technology was introduced. In fields such as aerospace, national defense, and shipbuilding, they are slowly taking the place of traditional high-strength steel and becoming a vital critical material [1–3]. The balance between strength and toughness becomes more challenging for steels with higher strength [4–6]. Currently, research on the performance enhancement of ultra-high-strength steel primarily focuses on improving the steel's microstructure and refining grain size. Kimura Y et al. [7] studied the mechanical properties such as strength, ductility, toughness, and resistance to the delayed fracture of ultra-fine grain martensitic high-strength steel and analyzed the effect of high-strength steel grain size on mechanical properties. Dolzhenko P et al. [8] analyzed the explanation for grain structure modifications in ultrafine-grained steel during plastic deformation. Li, JH et al. [9] provided a summary and discussed the main reasons behind the superior mechanical performance of three commonly used martensitic steels, as well as the strengthening/toughening mechanisms of the steels. In order to enhance the future application of ultra-high-strength steel, it is essential to strive for superior mechanical performance in a new and innovative direction. It is anticipated that the next generation of high-strength steel will demonstrate even better outcomes in machining and welding processes, which will be critical for its production applications [10,11].

Welding is a common method for connecting and processing ultra-high-strength steel. Despite this, it is facing multiple challenges in the current production processes. During the welding of ultra-high-strength steel with fine grain strengthening, the base material undergoes phase transformation and grain growth in the heat-affected zone. This leads to a significant reduction in the mechanical properties of the welded joint, as mentioned in references [12–15]. In addition, for steel with ultrafine-grained reinforcement, the welding heat input is bound to cause grain growth [16–18]. Moreover, because ultra-high-strength steel is highly durable and has a distinct grain structure, it can be challenging to control welding deformation, resulting in significant stress after the welding [19]. Therefore, when welding ultra-high-strength steel, it is essential to control welding deformation and residual stresses using pre-weld heating and heat treatment.

Sisodia R P S et al. [20] carried out a thorough investigation into the issue of heat-affected zone (HAZ) hardening of dual-phase (DP) steel during laser welding. They analyzed and compared the joint characteristics, microstructure, and mechanical properties of 1 mm thick dual-phase steel and evaluated the influence of post-weld heat treatment (PWHT) on the strengthening of laser-welded joints. Alipooramirabad H et al. [21] significantly reduced residual tensile stress in multi-pass high-strength steel welds using heat treatment. Often, relying on post-weld heat treatment to reduce weld residual stress is a time-consuming task. Furthermore, local treatment of larger structural components presents challenges that can limit the application of heat treatment [22].

Qi chao et al. [23] conducted various heat treatments on 316L austenitic stainless steel added and manufactured via a laser powder bed melting process for the first time to systematically study the evolution of residual stress, microstructure, and mechanical properties. During the laser additive manufacturing process, 316L stainless steel exhibited significant residual compressive stresses. After 2 h of post-treatment annealing at 400 and 650 °C and 5 min of solution annealing at 1100 °C, moderate to complete stress relief was achieved by 24%, 65%, and 90%, respectively. Chi et al. [24] utilized an integrated post-treatment process that involved heat treatment (HT) and laser shock peening (LSP) to alter the microstructure and mechanical properties of Ti17 titanium alloy. The results showed that the combined treatment of HT and LSP resulted in severe plastic deformation of the surface layer, leading to a high level of compressive residual stress on the surface. Meanwhile, after laser shock wave treatment, high-density dislocations and mechanical twins were observed in the rough phase, which gradually evolved into the fine phase. HT and LSP treatment ensured that the original ultimate tensile strength was maintained, but the sample's elongation was significantly increased by 15%.

In addition, Ji Xiangyu et al. [25] analyzed the formation and evolution mechanism of residual stress during the solid solution heat treatment process of 316L/Q235B composite plates and reduced the level of residual stress by improving the solid solution heat treatment process; Liu Zichen et al. [26] used simulation to elucidate the impact of post weld heat treatment differences on the relief effect of residual stress; B. Shakeri et al. [27] investigated the mechanism of the effect of cast iron phase transformation on residual stress under isothermal heat treatment; E. Heidari et al. [28] provided the possibility of improving the mechanical properties of materials via ablation and rolling methods.

The advantages of ultrasonic treatment include energy efficiency, high efficiency, and lightweight equipment over heat treatment methods. In the welding field, ultrasound is being applied and researched gradually. Feilong Ji et al. [29] coupled ultrasonic energy with the arc deposition process to study the effect of ultrasonic intensity on the microstructure and mechanical properties of ER70S-6 steel alloy during the direct energy deposition arc (DED-Arc) process. To analyze the propagation and vibration distribution of ultrasonic waves in the matrix, numerical simulation methods were employed. The study shows that increasing ultrasonic intensity expands the grain refinement area from the center of the melt pool to the surrounding area and alters the grain morphology from coarse columnar to fine equiaxed. In recent years, it has gradually become an ideal method for treating joints after welding. Applying ultrasonic impact treatment to both sides of the weld toe region can bring about several benefits. It can enhance the material's fatigue resistance, reduce stress concentration at the weld toe, and generate a compressive stress layer in the impacted area. This, in turn, can improve the microstructure near the surface of the impact location, as evidenced by research studies [30,31]. GRM Ali et al. [32] studied the influence of ultrasonic shot peening on the mechanical properties of TIG welded joints made of low-carbon steel. As the ultrasonic treatment intensity increased, the tensile strength of the welded joint showed a trend of decreasing at first and then increasing. Furthermore, the microhardness of the treated surface was elevated via ultrasonic treatment, causing a decrease in the weld's bending performance. ZhiQiang Liang et al. [33] made use of ultrasonic rolling to harden the surface of ultra-high-strength steel (45CrNiMoVA) while also investigating the progression of fatigue life on the surface of ultra-high-strength steel. The results show that ultrasonic rolling increased the residual compressive stress amplitude on the surface of ultra-high-strength steel, affecting the depth of the hardness layer and ultimately improving the material's mechanical properties.

As of now, the mechanical properties of newly developed ultra-high-strength steel have been constantly evolving. However, research on the development of welding processes for ultra-high-strength steel remains limited. Additionally, the main research direction to address problems such as easy deformation and excessive residual stress during the welding process is mainly focused on heat treatment methods. There is a relative lack of research on the improvement of weld microstructure and properties via ultrasonic treatment [34]. In the production of bulletproof vehicles, steel plates with a thickness of less than 6 mm are typically used and the welding method employed is segmented welding, which is fixed in advance by spot welding. Generally, the length of the welds is not more than 30 cm. Based on this, the size of the test steel plate is determined. The steel plate involved in this article is a new trial-produced steel plate and there is currently no model available. It has broad application prospects in protection due to its exceptional mechanical properties, making it of significant research value. The focus of this paper is on the newly developed ultrafine-grained high-strength steel that has a grade of 2000 MPa. The microstructure and properties of a MAG homogeneous weld joint were studied after applying ultrasonic treatment to the weld toe region. The purpose of this study was to provide a reference for welding production, as well as to eliminate residual stress and improve the mechanical properties of welds.

2. Experimental Procedure

The thickness size of the 2000 MPa ultra-high-strength test steel plate is 4 mm, which has extremely high strength and hardness. ER120S-G was used as the filler material. The chemical composition of the material is shown in Table 1. A butt joint with a total length of 200 mm was made using a traditional I-shaped groove following the American Welding Society [AWS: America, AWS D1.4/D1.4M-2005]. After thorough cleaning, the plates were securely clamped onto fixtures that were part of an automated welding platform. The 2000 MPa-grade ultra-high-strength steel is shown in Table 2 in terms of its mechanical properties.

Table 1. Chemical composition of 2000 MPa-UHSS.

Material	Chemical Composition/Wt. %										
	C	Co	Mn	Si	Cr	V	Mo	Ti	Ni	Ca	Al
2000 MPa-UHSS	0.36	0.006	0.18	0.102	1.116	0.005	0.268	0.065	0.018	0.072	0.072

Table 2. Mechanical properties of the welding materials.

Material	0.2% Yield Strength/MPa	Ultimate Tensile Strength/MPa	Elongation/%	Hardness Value/HV
2000 MPa-UHSS	1761.66 ± 21.4	2108.84 ± 18.6	10.35 ± 1.0	664.3 ± 17.3

The MAG welding method was used to connect the ultra-high-strength steel plates with 2000 MPa. The single-side welding and double-side forming technique was employed. The Fronius TPS5000B power supply was employed for welding and the KUKA 16 robot was used to automate the process. The weld seam had good formation and no visible defects on its surface. To ensure the accuracy of subsequent experiments, non-destructive testing was conducted on the weld using micro X-ray flaw detector XXG-2505 (Leeb, Chongqing, China). The results indicated that the weld quality was Level I.

Using the UIT-300 (EPT, Tianjin, China), ultrasonic impact treatment was applied to both sides of the weld toe region on both sides of the welded plates and on both the front and back. After ultrasonic treatment, the weld toe region showed varying degrees of concave deformation. To investigate the effects of ultrasonic treatment on the residual stress, surface microstructure, hardness, and tensile strength of 2000 MPa ultra-high-strength steel, samples were taken both before and after the treatment was applied to the weld seam. Following that, the impact of ultrasonic treatment on the microstructure and mechanical properties of welded joints was investigated. Table 3 provides detailed information on the automated welding process parameters and ultrasonic treatment parameters, while Figure 1 shows the experimental equipment and sampling positions.

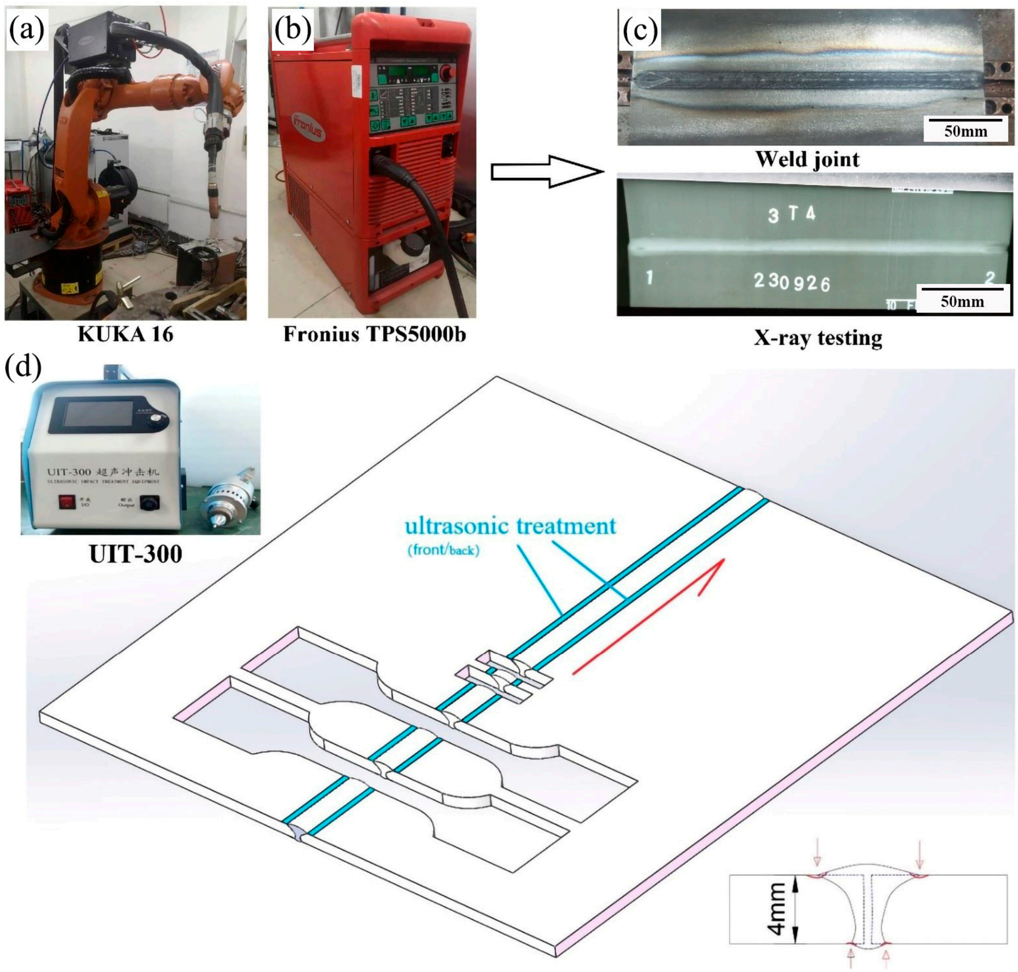

Figure 1. Experimental process and specimen cutting. Welding equipment includes (**a**) KUKA 16; (**b**) Fronius TPS5000b. After non-destructive testing (**c**) of the weld seam, (**d**) UIT-300 is used to perform ultrasonic treatment on both sides of the weld toe and samples are taken before and after treatment.

Table 3. Welding and ultrasonic treatment parameters.

Welding		**Current/A**	**Wire Feeding Speed/(m·min^{-1})**	**Voltage/V**	**Welding Speed/(m·min^{-1})**
		152	**0.7**	**23**	**0.35**
ultrasonic treatment	Number	Frequency/kHz	Speed/(mm·s^{-1})	Amplitude/μm	Probe diameter/mm
	1	10	3.5	25	3
	2	15			
	3	20			
	4	25			

3. Results and Discussion

3.1. Microstructure and Joint Morphology

The microstructure and joint morphology at various positions of the ultra-high-strength steel-welded joint are shown in Figure 2. The microstructure and grain size of the welded joint have changed significantly from the 2000 MPa-grade ultra-high-strength steel base material microstructure. Figure 2b shows that the weld seam area is primarily made up of lower bainite. Due to the ultra-high-strength steel base material's very small structure, the cooling process near the fusion line and the heat-affected zone is relatively slow, resulting in slight supercooling. In this scenario, a smaller degree of undercooling prevents the growth of a martensite structure near the fusion line in the weld area, resulting in a dominated weld structure made up of fine bainite. In addition, the low degree of supercooling causes the weld area to be dominated by equiaxed grains and the central structure of the weld to have no specific grain growth direction. In the area near the fusion line, some dendrites grew perpendicularly to it and the grain size was significantly larger than in the central area.

As the temperature increases, the ultra-high-strength steel's fine-grained structure gradually transforms into austenite near the fusion line on the side of the heat-affected zone, as shown in Figure 2c. The removal of the welding heat source results in rapid cooling, leading to the formation of significant coarse lath martensites, as demonstrated in Figure 2d. Due to this, the hardness in this area could be significantly higher than in the weld seam area. Unlike traditional high-strength steel, the experimental steel grade hardly forms a widmanstatten structure in the coarse-grained heat-affected zone (CGHAZ). In the zone that is heat-affected closer to the weld (Figure 2e), the heat input is less, resulting in a lower temperature gradient experienced by the grains during phase transformation. This leads to the formation of smaller martensitic grain structures. Also, there is less residual tensile stress generated beyond the weld seam. The grain's distortion and stretching degrees are not as significant as they are in the proximity of the weld, which also reduces grain growth.

As the distance from the weld seam increases, changes in the microstructure of the base material can be observed in the intermediate critical heat-affected zone (ICHAZ) of the joint (Figure 2f). The heating temperature in this area is not sufficient to initiate the transformation of the austenite phase in the base material. Tempering is the only process the base material undergoes, which results in a slight increase in grain size. At the grain boundaries, carbide precipitation also happens.

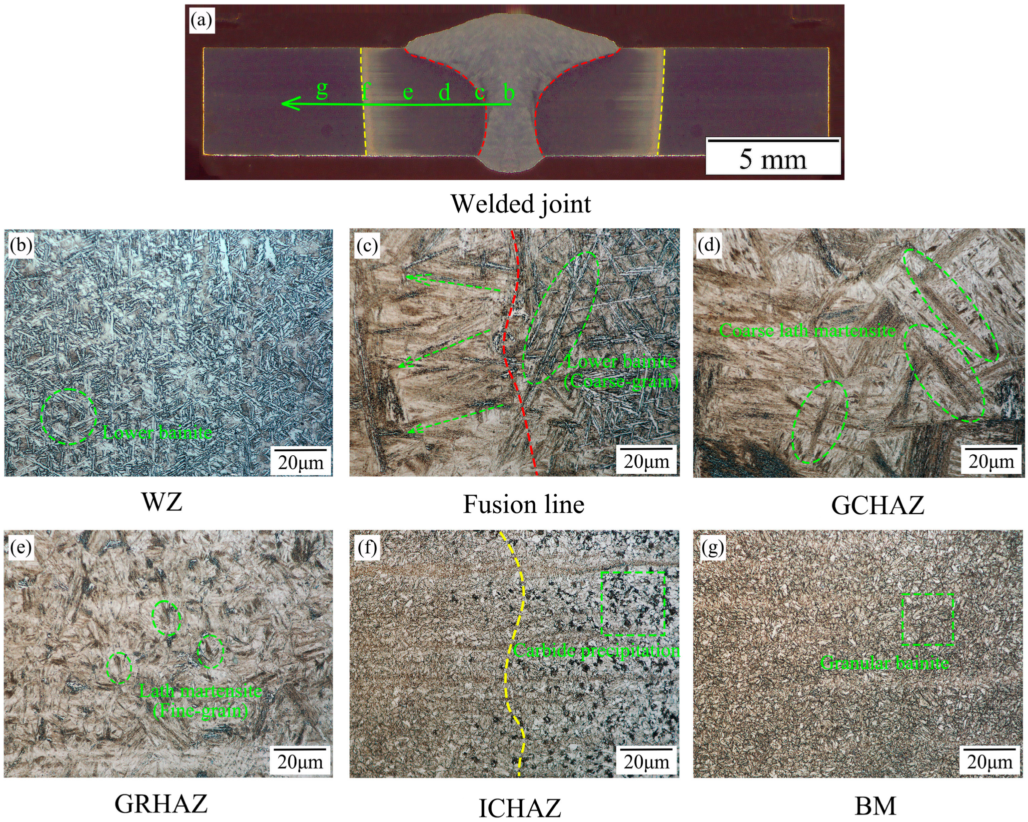

Figure 2. Metallographic structure of welding joints of UHSS. The boundary between the WZ, HAZ, and BM structure is clearly visible in the (**a**) macroscopic metallography. As the distance from the weld increases, the microstructure and grain size of the welded joint undergo significant changes (**b**–**g**). The microstructure of the WZ is dominated by lower bainite and the HAZ is dominated by lath martensite.

The weld toe regions on both sides of the weld experience changes in joint morphology after applying ultrasonic treatment, as shown in Figure 3. Ultrasonic treatment results in a noticeable concave deformation of the weld toe region. Gradually increasing the treatment frequency causes the concave deformation at the weld toe region to become more pronounced. Due to the formation of a significant amount of lath martensite and the increase in grain structure, the ductility of HAZ is reduced compared to the base material and weld. The primary concentration zone for residual tensile stresses is also located in this area. Upon increasing the treatment frequency to 25 kHz, both sides of the concave curve formed by the impact exhibit outward deformation of the weld metal and some areas show tiny cracks. Excessive ultrasonic frequency can lead to the destruction of the surface structure of the weld, which in turn affects the mechanical properties of the joint [35].

Ultrasonic treatment of high-strength steel is accomplished using an ultrasonic probe with a diameter of 3 mm. At the processing location, concave deformation occurred after the weld toe was applied to the joint continuously and appropriately using an ultrasonic probe. Therefore, its essence is extrusion deformation and appropriate impact can compact defects such as shallow cracks and pores on the surface of the weld seam, improving the surface flatness at the weld toe position. At the same time, it is essential to control the plastic deformation that occurs during the extrusion process. Moreover, the weld toe region is within the coarse-grained heat-affected zone, which has a higher stiffness level, a coarser grain composition, and a lesser grain boundary area. Under ultrasonic treatment, plastic deformation is limited, and the surface is susceptible to extrusion cracks.

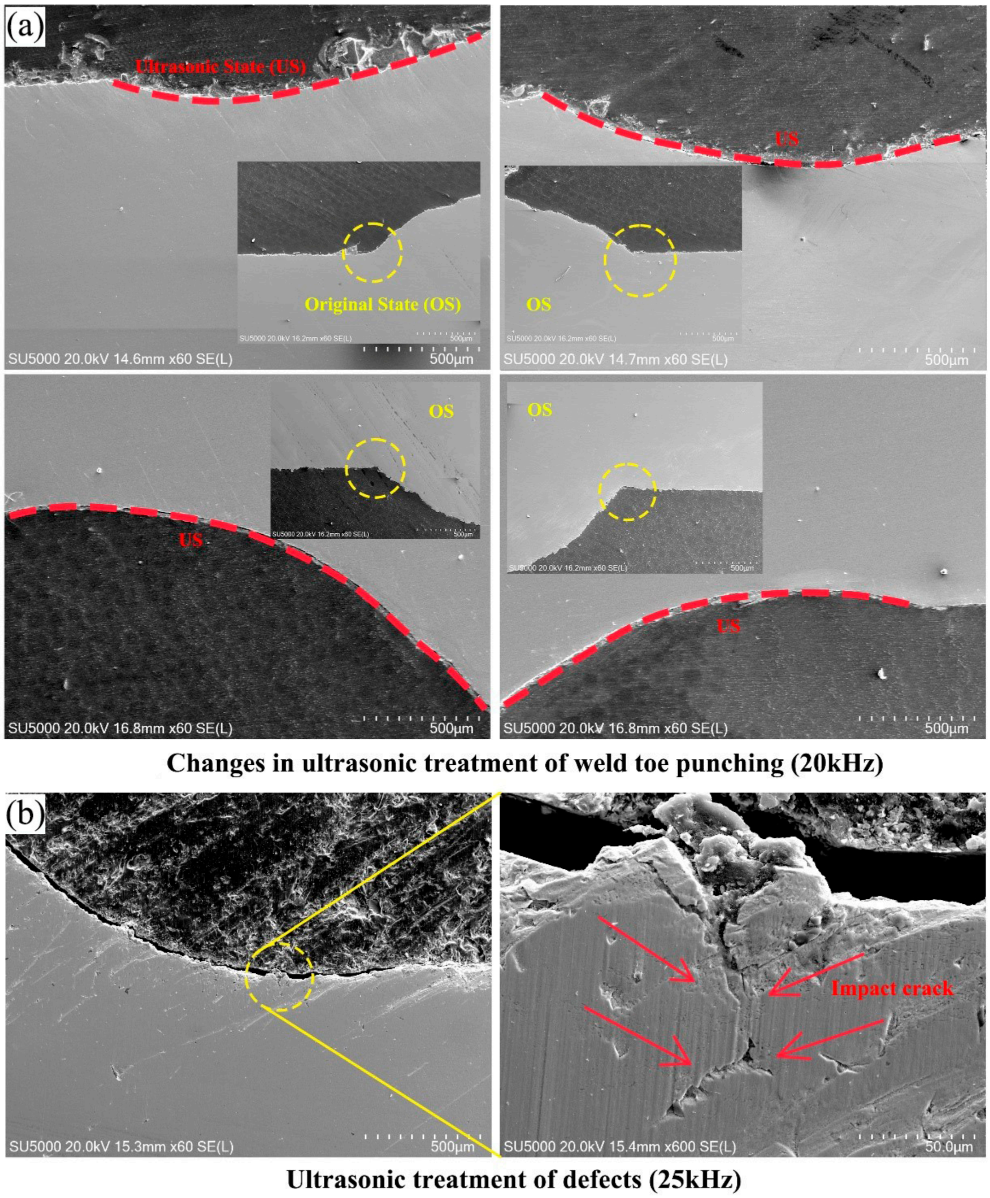

Figure 3. Surface deformation and crack defects of weld toe under SEM. Under ultrasonic treatment, the surface of the weld toe undergoes concave deformation (**a**). When the ultrasonic treatment frequency reaches a certain value (25 kHz), small impacting cracks appear on the treated surface (**b**).

The microstructural changes at the weld toe region after ultrasonic treatment are depicted in Figure 4. Plastic deformation is evident on the weld toe surface after the 20 kHz ultrasonic treatment. Despite the microstructure becoming more refined and uniform, the surface oxide film layer of the weld seam remains intact. Significant changes have been made to the grain arrangement and orientation in the weld seam area, resulting in a lot of grain boundary dislocations [36]. There is a smoother flow between the weld seam region and the heat-affected zone. In addition, carbide precipitation is found at the grain boundaries in the plastic deformation region after the ultrasonic impact. These factors together contribute to an increase in microhardness in the treated surface layer [37].

In previous studies on the impact of ultrasonic treatment on the microstructure of lightweight materials, it was found that high-frequency ultrasonic treatment may cause tissue damage to lightweight carbides [38]. To investigate whether ultrasonic treatment has caused changes in the microstructure of the weld seam, XRD phase detection was performed on the surface of the treated weld toe. Detection position 1 is the weld seam area, and detection position 2 is the fine-grained layer. The inspection results indicated that the phase structure of the weld zone remained unchanged after ultrasonic treatment. Combining metallographic analysis, the microstructure of the weld seam is mainly bainite (110), with a small amount of the Co_3Fe_7 phase (200) and the Ni·Cr·Fe (211) compound generated. After ultrasonic treatment, the fine grain layer on the weld toe surface underwent grain refinement without undergoing phase transformation.

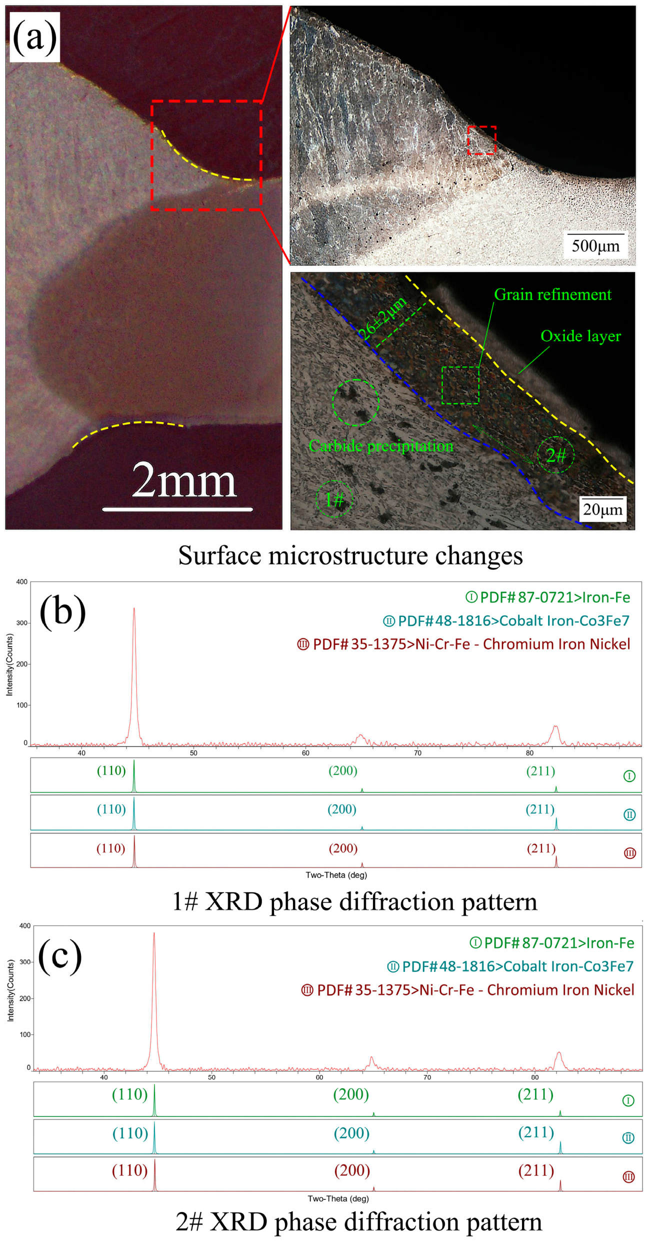

Figure 4. The metallographic changes on the surface of the weld toe and the XRD phase detection pattern. After ultrasonic treatment, the surface structure of the weld toe undergoes grain refinement (**a**). The XRD results showed that there was no significant change in the microstructure of the fine grain layer (**b**,**c**).

3.2. Residual Stress

Residual stress testing was carried out at the midsection of the ultra-high-strength steel weld, four millimeters from the weld seam, before and after ultrasonic treatment. Figure 5a shows the locations where the strain gauge is placed during residual stress testing. The ultrasonic treatment frequencies of 10 kHz, 15 kHz, 20 kHz, and 25 kHz were used to measure residual stress values near the weld. This aimed to investigate the effect of frequency on the elimination of residual tensile stresses in the welded joint.

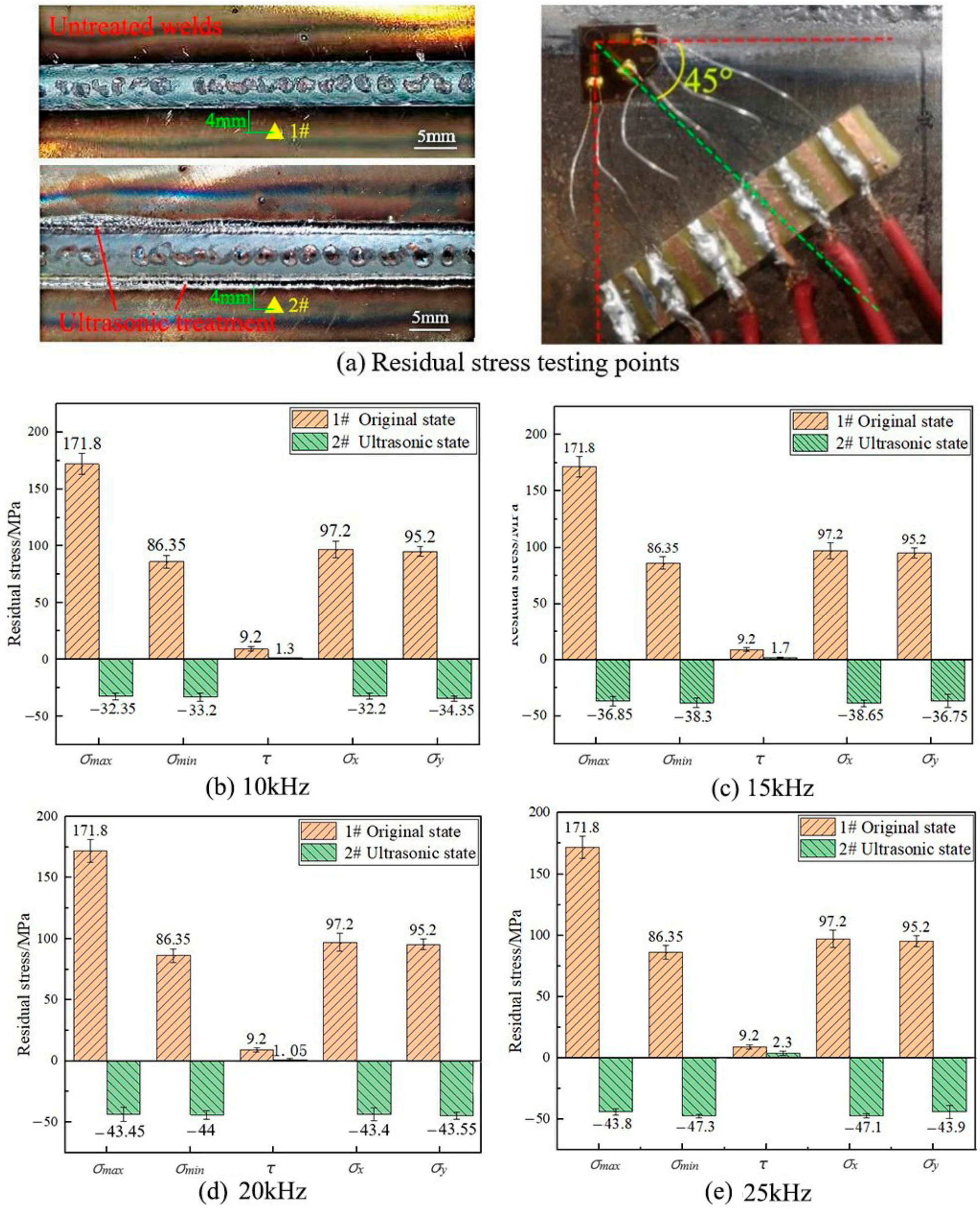

Figure 5. The effect of ultrasonic treatment on residual stress in welds. The measurement point is located at a distance of 4 mm from the middle section of the weld seam (**a**). After ultrasonic treatment, the residual stress distribution of the welded joint is more uniform and the residual stress changes from tensile stress to compressive stress (**b**–**e**).

Figure 5b–e presents the comparison between the residual stresses of the original and ultrasonic-treated welds. The weld's initial state has an average maximum residual stress of 171.8 MPa and an average minimum residual stress of 86.35 MPa. Compared to σ_x and σ_y, the shear stress values measured around the weld seam were smaller, approximately 10% of σ_x and σ_y. It can be concluded that the 4 mm thick ultra-high-strength steel plate filled with ER120S-G wire experienced minimal plastic deformation following welding. Based on the original welding data, it was discovered that there is a notable disparity in the extreme residual stress levels present in the welded joints. The average values of maximum and minimum residual stresses differ greatly and the residual stress is mainly residual tensile stress.

After ultrasonic treatment, the residual stresses in the welded joint gradually decreased. The residual tensile stresses in the welded joint were transformed into compressive stresses, which enhanced the joint's deformation resistance. Furthermore, the welded joint's distribution of compressive stresses was improved via ultrasonic impact, leading to a more uniform stress concentration in the joint. With the continuous increase in ultrasonic treatment frequency, the residual compressive stress values generated in the welded joint have also gradually increased. At approximately 20 kHz, the ultrasonic frequency caused the rate of increase in residual compressive stress to slow down and stabilize, ultimately resulting in a residual stress value of around 45 MPa.

Upon review of the relevant literature, it was discovered that both the initial residual tensile stresses and the residual tensile stresses caused by ultrasonics were comparatively low compared to traditional high-strength steel. This is due to the ultrafine grain structure in ultra-high-strength steel. This structure enhances the release of residual stresses after welding, resulting in lower residual tensile stresses compared to traditional high-strength steel. Moreover, when the weld seam undergoes deformation due to impact, it produces residual compressive stress. In such a scenario, the fine-grained structure plays a significant role in absorbing the impact and the larger grain boundary area provides more space for grain movement during deformation. This results in the residual compressive stress value of ultra-high-strength steel after treatment being lower than that of traditional high-strength steel.

3.3. Hardness

Figure 6 displays the Vickers hardness measurement locations and microhardness distribution of the welded joint at different ultrasonic treatment frequencies. The microhardness measurement load is set to 500 g and the load holding time is 10 s. The results of the microhardness test reveal that the hardness of the weld seam, coarse-grained heat-affected zone, and fine-grained heat-affected zone of the welded joint is significantly affected by the ultrasonic treatment.

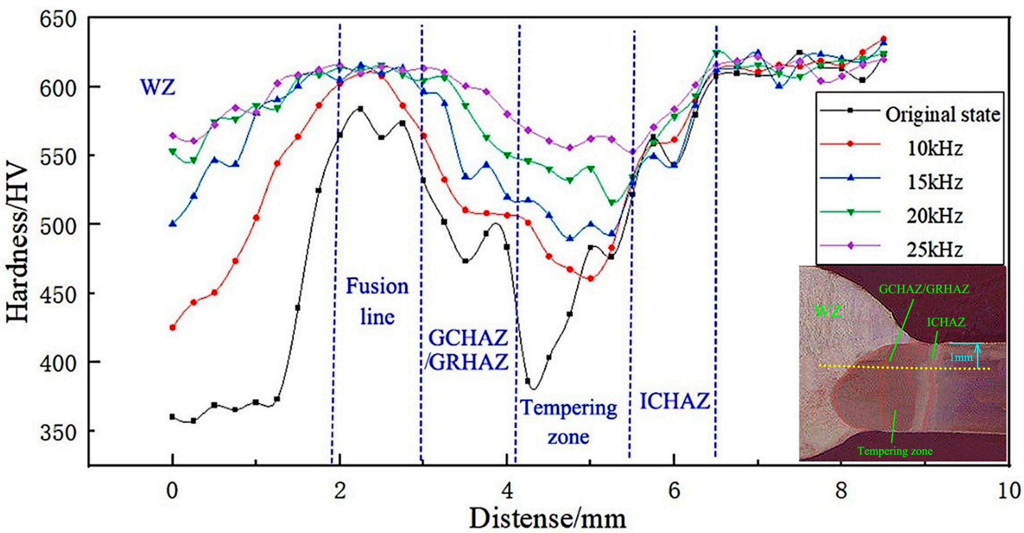

Figure 6. Microhardness distribution of welded joints under four different ultrasonic treatment frequencies (10 kHz, 15 Hz, 20 kHz, and 25 kHz). As the frequency of ultrasonic treatment increases, the average hardness of the joint significantly increases. The maximum microhardness appears in the fusion line zone (around 620 HV), while the minimum microhardness appears in the tempering zone (355 HV~375 HV).

The hardness test of welded joints is conducted in the horizontal direction of the cross section. Due to the symmetrical distribution of the joint structure, the hardness test is only conducted on one side of the welded joint. The microhardness testing points are shown in Figure 6. The hardness line is located 1 mm from the surface of the base metal and passes through the weld zone, fusion line, CGHAZ, GRHAZ, ICHAZ, and ultra-high-strength steel base metal in sequence.

The welded joint in the original state has significant differences in hardness at different locations. The structure of the central weld area is mostly lower bainite, and the microhardness is between 355 and 375 HV. A large hardness gradient is formed by the sharp increase in hardness of the weld area near the fusion line. The reason for this is that the temperature at the peak of the thermal cycle is the highest on both sides of the fusion line. As a result, the cooling rate is faster, which leads to a relatively coarse, entangled grain structure. Additionally, a significant amount of high-hardness lath martensite is produced on one side of the base metal. The combination of these factors leads to a high hardness on both sides of this area, of which the microhardness measurement in this area is between 550 and 570 HV. With increased distance from the weld, the size of the martensite grain with a lathed shape decreases gradually. In most cases, a decrease in grain size leads to an increase in hardness. However, the relatively low cooling rate caused by being far away from the weld seam also delays the occurrence of martensitic phase transformation, thereby producing other low-hardness phase structures such as bainite in the heat-affected zone, resulting in a gradual decrease in the hardness of the heat-affected zone. The hardness of the heat-affected zone near the tempering zone has been reduced to about 400 HV. There is a lack of high-hardness phase structure in the tempering zone, which results in a low thermal cycle peak temperature. Compared to the structure of the base metal, only a small amount of grain growth and carbide precipitation occurred in the tempered zone. The hardness of this area dropped below that of the base metal because of grain growth and the precipitation of carbides did not stop it from happening. The minimum hardness in the tempering zone is about 380 HV and, as the influence of the welding thermal cycle decreases, the grain growth in the tempering zone decreases and the hardness gradually increases. Near the critical heat-affected zone, the joint hardness has reached 90% of the hardness of the base metal.

The hardness distribution of the welded joint changed significantly after being treated with ultrasonics. First, under the ultrasonic treatment frequencies of 10 kHz, 15 kHz, 20 kHz, and 25 kHz, the overall hardness of the welded joints increased significantly. The highest level of hardness in the welded joints for all four ultrasonic frequencies occurs in the fusion line area, just below the ultrasonic impact weld toe. The maximum hardness is around 620 HV. The study revealed that the 10 kHz ultrasonic frequency has a significant impact on the hardness of welded joints up to a depth of 1 mm. Moreover, as the ultrasonic frequency increases, the depth at which the maximum hardness occurs also increases. However, the maximum hardness remains unchanged. In the weld zone, when the processing frequency reaches 20 kHz, the peak hardness of the welded joint no longer increases. At this time, the hardness of the central weld area is approximately 560 HV and gradually increases to approximately 620 HV as it approaches the fusion line. When the processing frequency is lower than 20 kHz, as the ultrasonic processing frequency increases, the hardness gradient in the weld area gradually decreases; thus, the hardness distribution becomes more uniform and gentle.

The hardness gradient in the heat-affected zone is reduced by applying ultrasonic treatment, which eliminates the difference in hardness values caused by grain size variations between coarse and fine-grain zones. As the frequency of ultrasonic treatment increases, the hardness of the heat-affected zone significantly increases. At 25 kHz, the hardness of the heat-affected zone is higher than 550 HV during treatment. The hardness alteration in the tempering zone is in line with that in the heat-affected zone. Ultrasonic treatment has little effect on the hardness of the critical heat-affected zone and the area near the substrate, with no significant change in hardness.

To sum up, the welded joint's overall hardness increases significantly after ultrasonic treatment, the hardness gradient is reduced, and the joint hardness distribution becomes more uniform. Further analysis of the impact of ultrasonic treatment on joint hardness: The change in the hardness of welded joints mainly depends on the response of the grain size and microstructure to ultrasonic impact. According to the tissue analysis in Figure 4, ultrasonic treatment does not cause major changes in the tissue morphology and grain size at the hardness measurement location. When it comes to tissue morphology, structures with high hardness are more resistant to plastic deformation and their hardness remains constant. However, low-hardness areas such as weld areas and fine-grained heat-affected zones undergo significant hardness increases due to compaction caused by ultrasonic treatment. Similarly, the grain size also responds to sonication. Compared to the coarse-grained region, under the same treatment frequency, the grain boundary area of the fine-grained region is larger, leaving more space for the formation of dislocations and slips. This is reflected in the change in hardness value, with a greater increase in hardness in the fine-grained area.

3.4. Tensile Strength

Tensile tests were conducted on the welded joints treated with an ultrasonic frequency of 20 kHz and the results were compared with those of the samples in their original state. Figure 7 depicts the locations of failure and fracture before and after ultrasonic treatment. The fractures occurred in the welding zone, along the centerline of the weld. A preliminary analysis of the fracture surfaces of the tensile samples before and after ultrasonic treatment reveals that the original-state weld fracture surface is relatively smooth with a stepped pattern. In contrast, the fracture surface of the state that was treated with ultrasonics has distinct granular structures. Both before and after ultrasonic treatment, there are evident tearing surfaces around the fracture surface, and the fracture surface in the ultrasonic-treated state shows a slight necking.

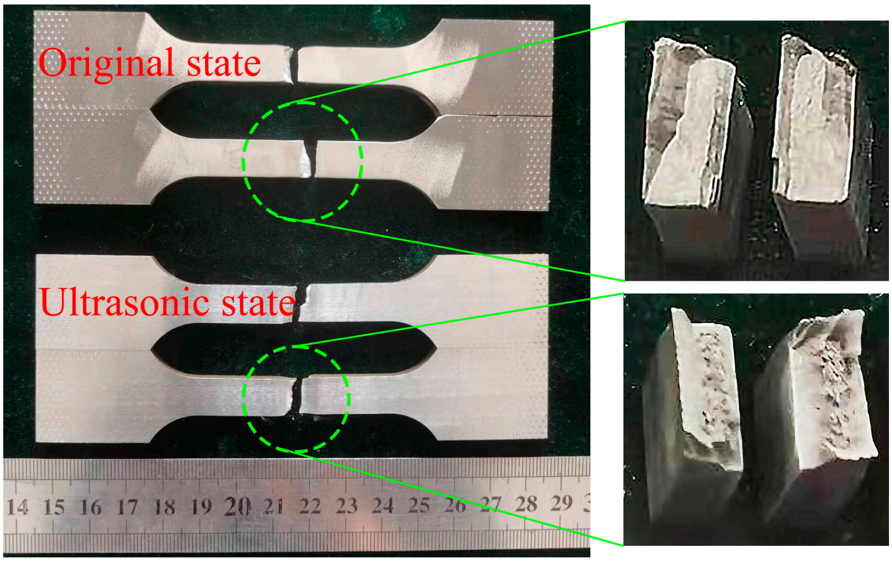

Figure 7. Fracture location of tensile specimen. The fracture necking of the ultrasonic-state sample is more pronounced than that of the original-state sample.

Figure 8 shows the stress–strain curves and test data that are associated with the tensile samples. In the original state, the yield strength and tensile strength of the weld seam are between 960~1005 MPa and 1170~1250 MPa, respectively. Additionally, the fracture elongation is around 2% (1#, 3#). After ultrasonic treatment with a frequency of 20 kHz, the ultrasonically treated sample 2# and sample 4# showed improved mechanical properties. Among them, the yield strength of the ultrasonic tensile specimen is increased to 1080~1120 MPa, and the ultimate tensile strength is increased to 1280~1370 MPa (2#, 4#). In addition, the fracture elongation of welded joints has been improved.

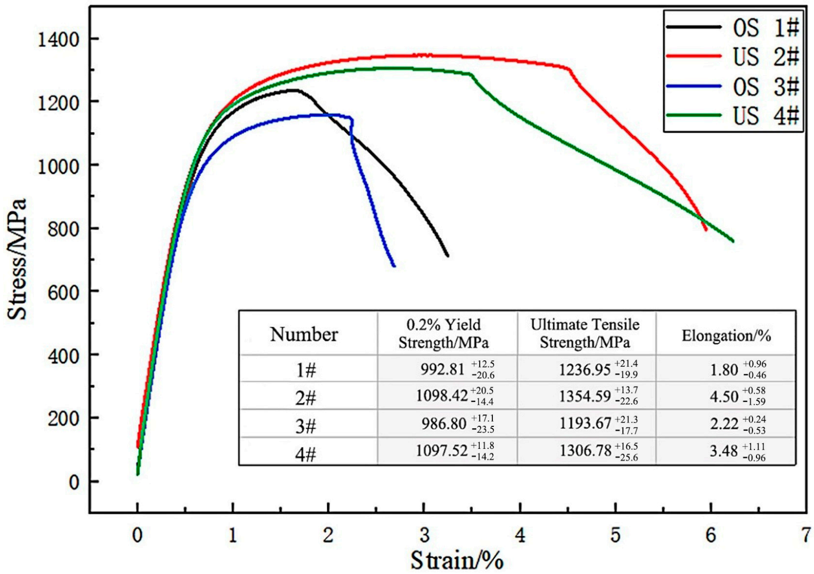

Number	0.2% Yield Strength/MPa	Ultimate Tensile Strength/MPa	Elongation/%
1#	$992.81^{+12.5}_{-20.6}$	$1236.95^{+21.4}_{-19.9}$	$1.80^{+0.96}_{-0.46}$
2#	$1098.42^{+20.5}_{-14.4}$	$1354.59^{+13.7}_{-22.6}$	$4.50^{+0.58}_{-1.59}$
3#	$986.80^{+17.1}_{-23.5}$	$1193.67^{+21.3}_{-17.7}$	$2.22^{+0.24}_{-0.53}$
4#	$1097.52^{+11.8}_{-14.2}$	$1306.78^{+16.5}_{-25.6}$	$3.48^{+1.11}_{-0.96}$

Figure 8. The effect of ultrasonic treatment on the tensile strength of welds. Ultrasonic treatment improves the tensile properties of welded joints.

The refinement of the surface grain structure in the welded joint after ultrasonic treatment is responsible for this enhancement. Increased grain boundaries allow the welded joint to withstand greater tensile strength due to higher deformation resistance. In addition, on the premise that ultrasonic treatment does not cause surface cracks, the grain boundaries in large areas provide more cushioning for deformation, thereby improving the fracture elongation of the ultrasonic-treated sample. In low-speed tensile experiments, the residual compressive stress generated via ultrasonic treatment could also enhance the tensile properties. Compressive stress around the ultrasonic weld is generated as previously mentioned and distributed evenly, leading to a decrease in local stress concentration. In addition, appropriate compressive stress can improve the plastic deformation ability of the material, which may also be an important factor in the significant increase in the elongation at the break of ultrasonic tensile specimens.

Figure 9 depicts the SEM images of the fracture surfaces of the tensile samples. As mentioned earlier, the fracture surface of the original tensile sample in the original state appears relatively smooth, with only a few fine cracks observed due to hydrogen embrittlement. Under scanning electron microscopy, it is possible to observe a quasi-cleavage fracture characteristic of hydrogen embrittlement. In contrast, the tensile sample that was treated with ultrasound has a transgranular ductile fracture morphology. The fracture surface exhibits a dense distribution of small dimples, with dimple sizes around 3 μm.

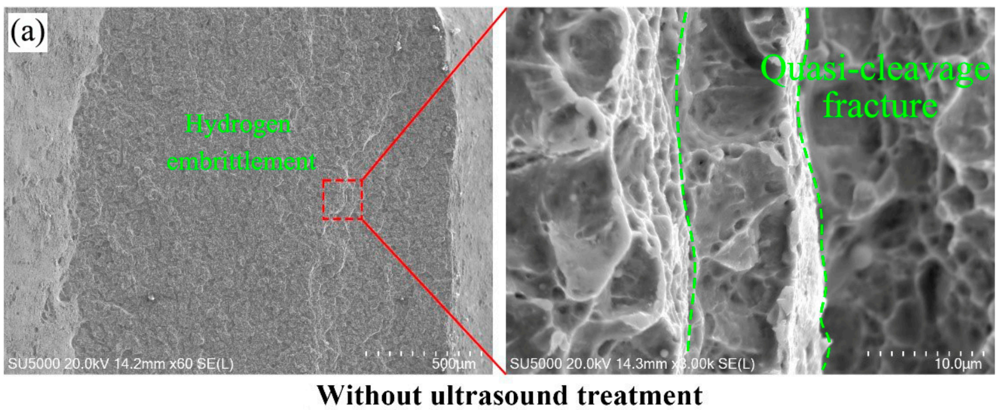

Figure 9. *Cont.*

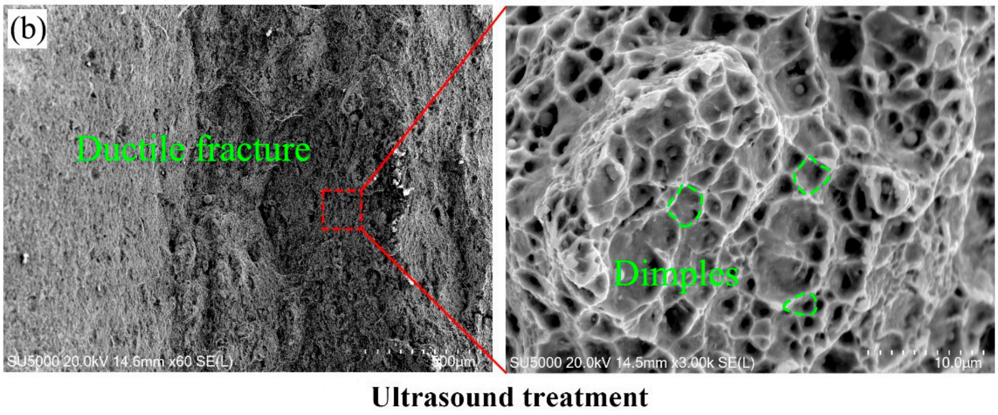

Figure 9. Fracture morphology of tensile specimens under SEM. The tensile fracture of the original-state sample exhibits quasi-cleavage fracture characteristics caused by hydrogen embrittlement (**a**), and a large number of small dimples were observed on the fracture surface of the ultrasonic-state sample (**b**).

4. Conclusions

In this study, MAG welding was used to join ultra-high-strength steel with a grade of 2000 MPa. The impact of ultrasonic treatment on the morphology, microstructure, residual stresses, and mechanical properties of the weld joint was investigated. The weld toe area was treated with ultrasonics, which created a fine-grained layer on the treated surface. The residual stress test results showed that ultrasonic treatment eliminated the residual tensile stresses on both sides of the weld, thereby generating compressive stresses. Hardness and tensile test results indicate that ultrasonic impact enhances the mechanical properties of the welded joint. As follows are the specific conclusions:

(1) The ultrasonic treatment exerted a compressive effect on the weld toe, creating a smooth transition at the weld toe. However, excessively high ultrasonic frequencies led to the generation of fine cracks in the treated surface. After ultrasonic treatment, a fine-grained layer was created on the treated surface, which refined the original grain structure of the weld region. Additionally, the grain orientations were changed and a small quantity of carbides formed in proximity to the fine-grained layer in the weld region.

(2) Ultrasonic treatment effectively eliminated the residual tensile stresses on both sides of the weld, inducing compressive stresses and enhancing the reliability of the welded joint. As the frequency of ultrasonic treatment increased, the hardness of the weld region and the coarse/fine-grained heat-affected zone also increased. The frequency needed to achieve peak hardness in the fusion line region was not very high. Increasing the treatment frequency widened the high-hardness zones on both sides of the fusion line and reduced the hardness gradient, resulting in a more uniform and gradual hardness distribution.

(3) The ultrasonic-state tensile samples showed a significant increase in yield strength compared to the original state. The grain refinement caused by ultrasonic treatment had a positive impact on the fracture elongation of the tensile specimens. Scanning electron microscopy images revealed distinct fracture characteristics between the original-state and ultrasonic-state specimens. In the original state, the joint specimen displayed a quasi-cleavage fracture morphology, with fine cracks of hydrogen embrittlement observed on the fracture surface. On the other hand, the ultrasonic specimen displayed a pronounced ductile fracture characteristic, with numerous small dimples observed on the fracture surface.

Lastly, the main focus of this study is on how ultrasonic treatment affects the surface microstructure and mechanical properties of the steel weld seam. There were no mentions of any other properties of the steel, such as corrosion resistance, magnetic resistance, and impact performance. The study of the impact of ultrasonic treatment on ultra-high-strength steel welds requires more research on the missing parts.

Author Contributions: Conceptualization, X.X. and Q.C.; methodology, Q.C.; validation, R.Y., X.X. and Q.C.; formal analysis, X.X.; investigation, Q.C.; resources, Q.C.; data curation, G.W.; writing—original draft preparation, X.X.; writing—review and editing, X.X.; visualization, G.W.; supervision, G.W.; project administration, Q.C.; funding acquisition, Q.C. All authors have read and agreed to the published version of the manuscript.

Funding: This research was funded by the National Key R&D Plan Project. (Project No. 2019YFB1900900).

Institutional Review Board Statement: Not applicable.

Informed Consent Statement: Not applicable.

Data Availability Statement: Data are contained within the article.

Conflicts of Interest: The authors declare no conflict of interest.

References

1. Ren, S.; Ma, N.; Tsutsumi, S.; Watanabe, G.; He, H.; Cao, C.; Huang, L. Post-weld cold working for fatigue strength improvement of resistance spot welded joint of advanced high-strength steel. *J. Mater. Process. Technol.* **2022**, *299*, 117364. [CrossRef]
2. Deng, Z.; Huang, S.; Wang, Y.; Xue, H. Experimental research on fatigue behavior of prestressed ultra-high performance concrete beams with high-strength steel bars. *Structures* **2022**, *43*, 1778–1789. [CrossRef]
3. Zhong, L.; Wang, B.; Hu, C.; Zhang, J.; Yao, Y. Hot Deformation Behavior and Dynamic Recrystallization of Ultra High Strength Steel. *Met.-Open Access Metall. J.* **2021**, *11*, 1239. [CrossRef]
4. Wen, C.; An, J.; Ding, L.; Qiu, X.; Bai, S. Stress Corrosion Cracking of 23Co14Ni12Cr3Mo Ultra-High Strength Steel in 3.5% NaCl Solution under Constant Load Condition. *Int. J. Electrochem. Sci.* **2021**, *16*, 211051. [CrossRef]
5. Liu, D.; Wang, J.-G.; Wang, H.-P.; Hu, Y.; Rao, H.-D. Characterization of hot deformation behavior of 30Si2MnCrMoVE low-alloying ultra-high-strength steel by constitutive equations and processing maps. *J. Iron Steel Res. Int.* **2020**, *27*, 807–819. [CrossRef]
6. Ishikawa, N.; Toji, Y.; Hojo, T. Development of Ultra-High Strength Steel Sheet and Evaluation Method for Hydrogen Embrittlement Behavior. *J. Jpn. Weld. Soc.* **2019**, *88*, 41–44. [CrossRef]
7. Kimura, Y.; Inoue, T. Mechanical Property of Ultrafine Elongated Grain Structure Steel Processed by Warm Tempforming and Its Application to Ultra-High-Strength Bolt. *Tetsu-Hagane* **2019**, *105*, 127–145. [CrossRef]
8. Dolzhenko, P.; Tikhonova, M.; Odnobokova, M.; Kaibyshev, R.; Belyakov, A. Ultrafine-Grained Stainless Steels after Severe Plastic Deformation. *Metals* **2023**, *13*, 674. [CrossRef]
9. Li, J.; Zhan, D.; Jiang, Z.; Zhang, H.; Yang, Y.; Zhang, Y. Progress on improving strength-toughness of ultra-high strength martensitic steels for aerospace applications: A review. *J. Mater. Res. Technol.* **2023**, *23*, 172–190. [CrossRef]
10. Brabec, J.; Ježek, Š.; Beneš, L.; Kříž, A.; Majrich, P. Suitability Confirmation for Welding Ultra-High Strength Steel S1100QL Using the RapidWeld Method. *Manuf. Technol. Eng. Sci. Res. J.* **2021**, *21*, 29–36. [CrossRef]
11. Hietala, M.; Hamada, A.; Keskitalo, M.; Jaskari, M.; Kumpula, J.; Järvenpää, A. Microstructural Evolution and Tensile Strength of Laser-Welded Butt Joints of Ultra-High Strength Steels: Low and High Alloy Steels. *Key Eng. Mater.* **2021**, *883*, 250–257. [CrossRef]
12. Hietala, M.; Ali, M.; Khosravifard, A.; Keskitalo, M.; Järvenpää, A.; Hamada, A. Optimization of the tensile-shear strength of laser-welded lap joints of ultra-high strength abrasion resistance steel. *J. Mater. Res. Technol.* **2021**, *11*, 1434–1442. [CrossRef]
13. Maeda, K.; Sato, Y.; Suzuki, R.; Suga, T.; Tsukamoto, M. Laser lap joining of high-strength steel to aluminum with cold sprayed steel coating. *J. Laser Appl.* **2021**, *33*, 042017. [CrossRef]
14. Ma, Y.; Yu, Y.; Geng, P.; Ihara, R.; Maeda, K.; Suzuki, R.; Suga, T.; Ma, N. Fracture modeling of resistance spot welded ultra-high-strength steel considering the effect of liquid metal embrittlement crack. *Mater. Des.* **2021**, *210*, 110075. [CrossRef]
15. Chen, J.; Yang, Y.; Li, L.; Wang, Z.; Xiao, H.; Wei, Y.; Zhu, T.; Sun, H. Effects of Ti on Microstructure, Mechanical Properties and Corrosion Behavior of High-Strength Steel Weld Metals for Offshore Structures. *Int. J. Electrochem. Sci.* **2021**, *16*, 210825. [CrossRef]
16. Yang, X.-H.; Chen, X.-H.; Pan, S.-W.; Wang, Z.-D.; Chen, K.-X.; Li, D.-Y.; Qin, J.-W. Microstructure and mechanical properties of ultralow carbon high-strength steel weld metals with or without Cu-Nb addition. *Int. J. Miner. Metall. Mater.* **2021**, *28*, 120–130. [CrossRef]
17. Sato, Y.; Murakami, Y.; Satoshi, I.; Ishikawa, N. Critical Conditions of Cold Cracking in High Strength Steel Weld Based on the Local Stress Distribution and Hydrogen Accumulation. *Mater. Sci. Forum* **2018**, *941*, 153–157. [CrossRef]
18. Funakoshi, T.; Tanaka, T.; Ueda, S.; Ishikawa, M.; Koshizuka, N.; Kobayashi, K. Improvement in Microstructure and Toughness of Large Heat-Input Weld Bond Due to Addition of Rare Earth Metals and Boron in High Strength Steel. *Tetsu-to-Hagane* **2010**, *63*, 303–312. [CrossRef] [PubMed]
19. Szymczak, T.; Szczucka-Lasota, B.; Węgrzyn, T.; Łazarz, B.; Jurek, A. Behavior of Weld to S960MC High Strength Steel from Joining Process at Micro-Jet Cooling with Critical Parameters under Static and Fatigue Loading. *Multidiscip. Digit. Publ. Inst.* **2021**, *14*, 2707. [CrossRef]

20. Sisodia, R.P.; Gáspár, M.; Draskóczi, L. Effect of post-weld heat treatment on microstructure and mechanical properties of DP800 and DP1200 high-strength steel butt-welded joints using diode laser beam welding. *Weld. World* **2020**, *64*, 671–681. [CrossRef]
21. Alipooramirabad, H.; Paradowska, A.; Nafisi, S.; Reid, M.; Ghomashchi, R. Post-Weld Heat Treatment of API 5L X70 High Strength Low Alloy Steel Welds. *Materials* **2020**, *13*, 5801. [CrossRef] [PubMed]
22. Lee, S.-J.; Son, J.-T. Recovery of lithium hydroxide monohydrate from a nickel-rich cathode material by a novel heat-treatment process at a significantly low temperature. *Funct. Mater. Lett.* **2021**, *14*, 2150018. [CrossRef]
23. Chao, Q.; Thomas, S.; Birbilis, N.; Cizek, P.; Hodgson, P.D.; Fabijanic, D. The effect of post-processing heat treatment on the microstructure, residual stress and mechanical properties of selective laser melted 316L stainless steel. *Mater. Sci. Eng. A Struct. Mater. Prop. Misrostructure Process.* **2021**, *821*, 141611. [CrossRef]
24. Chi, J.; Cai, Z.; Wan, Z.; Zhang, H.; Chen, Z.; Li, L.; Li, Y.; Peng, P.; Guo, W. Effects of heat treatment combined with laser shock peening on wire and arc additive manufactured Ti17 titanium alloy: Microstructures, residual stress and mechanical properties. *Surf. Coat. Technol.* **2020**, *396*, 125908. [CrossRef]
25. Ji, X.; Zhao, Z.; Sun, C.; Liu, X.; Wang, R.; Su, C. Study on Residual Stress Evolution Mechanism and Influencing Factors of 316L/Q235B Composite Plate during Solution Heat Treatment. *Crystals* **2023**, *13*, 436. [CrossRef]
26. Liu, Z.; Hu, X.; Yang, Z.; Yang, B.; Chen, J.; Luo, Y.; Song, M. Optimization Study of Post-Weld Heat Treatment for 12Cr1MoV Pipe Welded Joint. *Metals* **2021**, *11*, 127. [CrossRef]
27. Shakeri, B.; Heidari, E.; Boutorabi, S.M.A. Effect of Isothermal Heat Treatment Time on the Microstructure and Properties of 4.3% Al Austempered Ductile Iron. *Int. J. Met.* **2023**, *17*, 3005–3018. [CrossRef]
28. Heidari, E.; Mohammadzadeh, M.; Boutorabi, S.M.A. Hot Rolling of Thin-Wall Ductile Cast Iron Produced by Ablation Casting. *Int. J. Met.* **2023**, *17*, 1637–1649. [CrossRef]
29. Ji, F.; Qin, X.; Ni, M.; Hu, Z.; Wu, M. Effect of ultrasonic intensity on microstructure and mechanical properties of steel alloy in direct energy deposition-Arc. *Ultrasonics* **2023**, *134*, 107090. [CrossRef]
30. Wang, Y.; Brodusch, N.; Gauvin, R.; Lin, C.; Zeng, Y. Tetragonal reconstruction and monoclinic variants rearrangement during heat treatment in zirconia. *J. Am. Ceram. Soc.* **2022**, *105*, 5436–5447. [CrossRef]
31. Riipinen, T.; Pippuri-Mäkeläinen, J.; Que, Z.; Metsä-Kortelainen, S.; Antikainen, A.; Lindroos, T. The effect of heat treatment on structure and magnetic properties of additively manufactured Fe-Co-V alloys. *Mater. Today Commun.* **2023**, *36*, 106437. [CrossRef]
32. Ali, G.R.M.; Ridha, A.Z.; Sadeq, D.A.; Ebraheem, A.A.; Atta, A.S. Effect of Ultrasonic Peening on Mechanical Properties of Low Carbon Steel AISI 1020 TIG Welding Joints Process. *Int. J. Appl. Mech. Eng.* **2022**, *27*, 194–204. [CrossRef]
33. Liang, Z.; Li, Z.; Li, X.; Li, H.; Cai, Z.; Liu, X.; Chen, Y.; Xie, L.; Zhou, T.; Wang, X. Experimental study on surface integrity and fatigue life of an ultra-high strength steel by the composite strengthening process of pre-torsion and ultrasonic rolling. *Eng. Fail. Anal.* **2023**, *150*, 107333. [CrossRef]
34. Blatnická, M.; Šajgalík, M.; Sága, M.; Blatnický, M. Comparison of Residual Stress in High Strength Steel Sample before and after Laser Welding. *Manuf. Technol.* **2018**, *18*, 369–371. [CrossRef]
35. Qiu, Z.; He, A.; Shao, J.; Xia, X. Reduction of Residual Stress for High-Strength Low-Alloy Steel Strip Based on Finite Element Analysis. *Adv. Mater. Sci. Eng.* **2018**, *2018*, 8131909. [CrossRef]
36. Tian, Z.F.; Li, J.F.; Chen, Z.X.; Wang, Z.N. Effect of Process Conditions on Residual Stress in Laser-MAG Welding of High Strength Steel. *Key Eng. Mater.* **2020**, *831*, 71–77. [CrossRef]
37. Yang, B.; Zhu, Q.; Nie, S.; Elchalakani, M.; Xiong, G. Experimental and model investigation on residual stresses in Q460GJ thick-walled I-shaped sections. *J. Constr. Steel Res.* **2018**, *145*, 489–503. [CrossRef]
38. Akhavan, O.; Ghaderi, E.; Akhavan, A. Size-dependent genotoxicity of graphene nanoplatelets in human stem cells. *Biomaterials* **2012**, *33*, 8017–8025. [CrossRef]